Effect of autopilot modes on flight performances of electric mini-UAVs

G. Guglieri
giorgio.guglieri@polito.it
Politecnico di Torino
Dipartimento di Ingegneria Meccanica e Aerospaziale
Italy

ABSTRACT

Great attention is focused on the development of both remotely controlled and unmanned flying vehicles. As a matter of fact, the design of such vehicles is a topical direction of development for modern aeronautics. Among such promising flying vehicles, micro- and mini-UAVs play a leading role. The present paper proposes a method to validate the inclusion of the relevant modelling elements in a comprehensive simulation tool reproducing some of the flight phases of a mini-UAV. The energy balance budget and the dynamic response of the aircraft during the automatic flight are investigated, assessing the impact of autopilot configuration, such as altitude-airspeed holding modes and suggesting a setting guideline for flight mode selection compatible with the features of commercial autopilots.

NOMENCLATURE

C	battery charge (Ah)
C_0	nominal battery charge (Ah)
e	error
E	energy (J)
h	altitude (m)
I	current (A)
I_0	no-load current (A)
I_S	stall current (A)

Paper No. 3777. Manuscript received 14 October 2011, revised version received 16 March 2012, accepted 12 April 2012.

K_D	derivative gain
K_I	integral gain
K_P	proportional gain
K_V	speed constant (rpm/V)
L, M, N	body-axes aerodynamic moment components at the centre of mass (Nm)
p, q, r	body-axes aircraft angular rates (rad/s)
Q	torque (Nm)
Qs	stall torque (Nm)
Re	Reynolds number
R_I	internal resistance (Ω)
S	wing surface (m^2)
t	time (s)
T	thrust (N)
V	voltage (V)
V_0	motor nominal voltage (V)
U	airspeed (ms^{-1} or alternatively Km/h)
W	weight (N or alternatively g)
X, Y, Z	body-axes aerodynamic force components (N)
α	angle-of-attack (deg)
β	angle of sideslip (deg)
χ	throttle setting (0:1)
δ_a	control surface deflection (aileron) (deg)
δ_e	control surface deflection (elevator) (deg)
Δt	integration time step (s)
ΔT	period (s)
η_M	efficiency (motor)
η_B	efficiency (battery)
η_C	efficiency (motor speed controller)
ε_I	current parameter
ε_h	altitude parameter
ε_U	airspeed parameter
ρ	air density (kg/m^3)
Ω	motor speed (rpm)
Ω_0	no-load speed (rpm)

1.0 INTRODUCTION

At present, great attention is focused on the development of both remotely controlled and unmanned flying vehicles. The creation of such vehicles is the topical direction of development of modern aeronautics. Among such promising flying vehicles, micro- and mini-UAVs play a leading role. These vehicles are very compact semi-autonomous flying robots with a fixed wing configuration. Rotary and flapping wing concepts were also widely implemented. The purpose of their missions is usually the surveillance of confined space. An extensive outline of the evolution of these flying platforms is given in Refs 1-6.

The main problem for the designer of these light weight autonomous vehicles is the very limited energy budget available. The estimation of steering and control losses through simulation i.e. the prediction of power consumed to climb and accelerate during the autonomous flight phases is

therefore a vital task in order to establish the mission range and endurance with accuracy. As usual in any aircraft design process, the inertial and aerodynamic properties of the vehicle play a role in the balance of forces and moments during the dynamics of flight. But the real issue is the estimation of the secondary contributors that enforce the accuracy of the performance analysis i.e. the propeller, the electric motor and the battery pack.

The details of propeller driven propulsion are very complex. Aircraft propellers convert motion from the rotary action of its motor to provide propulsive force. The engine needs to create a torque to rotate the propeller . Thus power created by the propulsion system is absorbed by the propeller and as a result thrust is generated. Model aircraft propellers are widely adopted for mini-UAVs: they are simple looking devices usually having no adjustable or moving parts. Propellers are described in terms of their diameter and pitch and the recommended pitch-to-diameter ratio for mini-UAVs is usually from 1:2 to 1:1. Nevertheless, with a too large pitch the propeller becomes inefficient at low forward speed and high rate as when during the take-off or climb. Whereas a propeller designed for good efficiency at take-off and during climb (with fine pitch and large diameter) will accelerate the aircraft very quickly from standstill but will reduce the top airspeed. Some propeller designs vary the pitch somewhat over the radius in an effort to improve the performance during some operational regime. Propeller performance at low Reynolds numbers has become increasingly important in the design and performance prediction of mini-UAVs. While propeller performance for full-scale aircraft has been well documented, data for propellers operating at low Reynolds numbers has been hardly available. The extension of conventional theories to this range of problems is far from immediate and some type of validation is required.

Finding the right electric motor is a complex task even if the brushless versions are the best option currently available for small scale UAVs. Efficiency is a measure of how much of the input power (the power that the battery delivers to the motor) is actually used to turn the propeller (output power) and how much is wasted as heat dissipation. A motor with higher efficiency delivers more power to the propeller and wastes less. Ultimately, a motor that is too small will overheat and damage itself while a motor that is too large will be a penalty to performance, due to its added weight. Translating propeller size and angular rate into power will also pass through some other alternative design options: battery voltage and capacity, direct drive or geared transmission, outrunner or inrunner motor. Though, the most important test to validate the analytical trade-off and the numerical simulations performed during the design phase still remains how the overall assembly performs in the air (flight test tuning).

Finally, the autopilot board is the most important and complex piece of hardware in the UAV system. The function of the autopilot is to control the aircraft using the aircraft states, the user-programmed mission and the pre-programmed fail-safe functions. The autopilot is a compact unit that contains: the processing unit, sensors to measure the aircraft states, input and output channels to govern the payload, GPS and serial modems, and auxiliary electronic components to support these devices. Another relevant technology segment is the software also providing the guidance, navigation and control functions. Several implementations are proposed either on the market or by specific developers. Anyway, a common feature is that the autopilot control system consists of conventional PID (Proportional-Integral-Derivative) loops

$$\Delta u = K_P e + K_I \int_0^t e(\tau)\mathrm{d}\tau + K_D \frac{\mathrm{d}e}{\mathrm{d}t} \qquad \ldots (1)$$

Therefore, tuning the PID values is very important to the performance of the UAV. The in-flight trail and error approach, based on empirical loop shaping methods and flight test experiments,

usually proposed as a first guideline by the autopilot manufacturers, is extremely time consuming. The correct tuning of control loops is a balance between aggressive suppression of tracking errors and minimisation of steering and control losses without excessive control compensation that may induce an oscillatory response. Furthermore, different altitude-airspeed holding modes are available as configuration options. The choice among the flight modes and their loop shaping is a balanced compromise of performances and it is closely cross-coupled with the behavior of servo actuators and propulsion system.

Hence, considering all the above mentioned issues, the objectives of this paper can be shortly summarised as:

1. To include the relevant modelling elements in a comprehensive simulation tool reproducing the flight mission of a mini-UAV.
2. To evaluate the fidelity of the simulation tool in terms of energy balance.
3. To analyse the dynamic response of the aircraft during the automatic flight phases assessing the impact of autopilot configuration.
4. To suggest a programming and setting guideline for low cost commercial autopilots.

2.0 SIMULATION MODEL

The simulations have been performed using a Fortran based software. The time domain response of the system is integrated with a Runge-Kutta explicit solver for ordinary differential equations based on Gill's fourth order method[10]. The time step is set as $\Delta t = 0{\cdot}001$s.

The aircraft motion is simulated by nonlinear force and moment equations (given in body axes) and by a set of kinematic equations for the Euler angles and the angular velocities. The aircraft rigid body model is detailed in terms of aerodynamic and propulsive actions.

The aerodynamic model (forces and moments) is introduced in the following form:

$$\begin{aligned} X &= X(\rho\, U, \alpha, q, \delta_e) \\ Y &= Y(\rho\, U, \beta, p, r, \delta_a) \\ Z &= Z(\rho\, U, \alpha, q, \delta_e) \\ L &= L(\rho\, U, \beta, p, r, \delta_a) \\ M &= M(\rho\, U, \alpha, q, \delta_e) \\ N &= N(\rho\, U, \beta, p, r, \delta_a) \end{aligned} \quad \ldots (2)$$

The aerodynamics of the vehicle were estimated numerically with a software tool (validated with wind-tunnel experimental data in Ref. 17) that implements the Weissinger theory[18] as an extension of the lifting line theory for swept wings[19].

The propulsion system (i.e. the thrust) is modeled as steady state subsystems: propeller, electric motor and batteries. Their dynamics is assumed to be at least one order of magnitude faster than the vehicle's response to commands (i.e. the propulsion system exhibits smaller time constants).

Propeller aerodynamics is implemented using the blade element theory corrected for inflow effects[11]. Blade aerofoil aerodynamics is generated with a Reynolds number dependent database. In this method (Glauert's theory) the propeller is divided into a number of independent sections along the length. At each section a force balance is applied involving 2D section lift and drag with the thrust and torque produced by the section. At the same time a balance of axial and angular

momentum is applied. This produces a set of non-linear equations that can be solved by iteration for each blade section. The resulting values of section thrust and torque can be summed to predict the overall performance of the propeller. The theory does not include secondary effects such as 3D flow velocities induced on the propeller by the shed tip vortex or radial components of flow induced by angular acceleration due to the rotation of the propeller. Given the above limitations it is still a low-computationally expensive tool available for getting first order predictions of thrust, torque and efficiency for propellers under a large range of operating conditions. An example of experimental validation (wind-tunnel experiments) for a reference propeller-motor combination (not adopted in the current case) is outlined in Fig.2.

The electric motor is represented as a system that converts electrical energy into mechanical energy and it is parameterised with no-load current I_0 and stall current I_S, nominal voltage V_0 and stall torque Q_S[12-13]:

$$\begin{cases} I_s = \dfrac{V_0}{R_I} \\ Q_s = \dfrac{I_S}{K_V} \\ \Omega = K_V V \end{cases} \quad \ldots (3)$$

and

$$\begin{cases} I = I_0 + \dfrac{I_S - I_0}{Q_S} \cdot Q \\ V = V_0 \cdot \left(\dfrac{\Omega}{\Omega_0} + \dfrac{Q}{Q_S} \right) \end{cases} \quad \ldots (4)$$

Hence, linear variation of torque Q with current I and angular rate Ω with voltage V is assumed. The efficiency of the motor is obtained as;

$$\eta_M = \frac{Q\Omega}{VI} \quad \ldots (5)$$

The batteries are modeled as an energy storage system whose capacity is limited by a discharge efficiency η_B that is a function of the discharge rate $n \cdot C$, a typical drawback of Lithium Polymer batteries:

$$C = \eta_B C_0 \quad \ldots (6)$$

For the present analysis the discharge efficiency $\eta_B = 92 \cdot 5\%$ equivalent to a $2C$-$5C$ discharge rate. The power loss due to the digital motor speed controller was also considered assuming $\eta_C < 99\%$ (representative of a 12kHz frequency switching voltage controller).

The implemented autopilot is a commercial multi loop PID autopilot (Micropilot MP2028[7] or equivalent). Capabilities include attitude holding, airspeed holding, altitude holding, turn co-

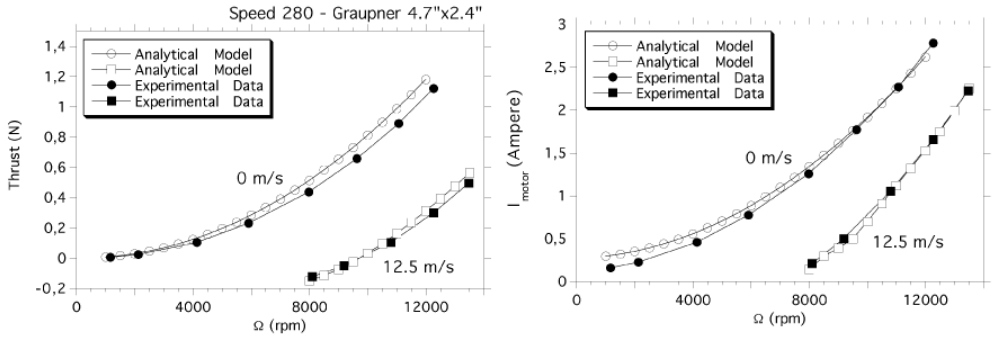

Figure 1. The experimental validation of the propeller-motor numerical model.

ordination and sequential GPS waypoint navigation. Flight control design of these light weight autopilots is usually based on conventional PID controllers since it is relatively straightforward to modify parameters in order to achieve the closed-loop specifications. The control gains and the simulator have been tested and experimentally validated using flight test data[8,9].

For the present analysis two different autopilot modes are considered: mode (1) in which elevator controls airspeed while throttle controls altitude and mode (2) that performs the opposite type of control. The update frequency of these control loops is $f = 5$Hz. Note that throttle χ and elevator δ_e are always related to each other so if one is controlling altitude h, the other implicitly controls airspeed U. There are advantages to each mode as declared by autopilot manufacturers[7]. If the elevator controls the altitude, then your autopilot will hold altitude with tighter tolerance and the throttle will have a more direct effect on airspeed U. If the elevator controls airspeed, then your autopilot will handle an engine failure more appropriately. This is much safer and it can avoid an undesired stall. These properties are the subject of the present investigation in order to define the impact of flight mode selection on a quantitative basis.

The control loops (mode 1 and 2) are tuned using the Tyreus and Luyben method that, differently from Ziegler-Nichols tunings, tends to reduce oscillatory effects and improves robustness[14].

3.0 DISCUSSION OF RESULTS

The present analysis is based on the simulation of the flight phases of a light weight fixed wing mini-UAV (MH850)[15-16] that has a wing span $b = 870$mm and a typical take-off mass of approximately 1,000g (see Fig. 2 and Fig. 3). It is a tailless integrated wing-body configuration with a single tractor propeller and the design has been developed for low-cost surveillance missions. The fuselage has a complex profiled shape. The swept wing has a moderate taper ratio without twist and dihedral. The wing aspect ratio is $\lambda = b^2/S = 3$ and the geometric sweep angle (referred to the wing leading edge) is $\Lambda = 25°$. Aircraft control is performed deflecting a pair of trailing-edge elevons (equivalent dual function as elevator and aileron). MH850 has enough specific excess power to climb with non-marginal rates at altitude. Only 45% of maximum power is required for low speed level flight at sea level. The longitudinal static stability of the aircraft was tuned after a specific flight test activity (the static margin – based on mean aerodynamic chord – is set at 10%). The thrust axis is aligned with the longitudinal body axis. A nose cone covers the front mounted electric motor. Removable panels give rapid access to components and the substitution of battery

packs is very simple and quick. Payload and autopilot are also readily accessible. The flight performances are: maximum airspeed $U \geq 20\text{ms}^{-1}$ (72km/h), cruise airspeed $U = 13{\cdot}5\text{ms}^{-1}$ (48km/h) and best sea level endurance $t_{BE} = 60\text{min}$.

The main characteristics of the propulsion system are hereafter shortly summarised: speed constant $K_V = 1{,}022\text{rpm/V}$, maximum power output 180w, internal resistance $R_I = 0{\cdot}109\Omega$, no-load current $I_0 = 0{\cdot}85\text{A}$ and $V_0 = 8{\cdot}4\text{V}$. The overall motor performance parameters (speed, efficiency, current and power output) are presented in Fig. 4 as a function of torque Q. The nominal capacity of the battery pack is $C_0 = 3{,}400\text{mAh}$ (3S1P LiPo). The propeller is a composite two-bladed commercial version for electric flight use with a diameter of 228·6mm and a geometric pitch of 15·24mm. The efficiency range of the propeller (for the considered flight regimes) is $\eta_P = 72 - 78\%$. The geometry (blade chord and twist) and the aerofoil aerodynamics of the propeller (the database is defined for $\alpha = -20° \div +60°$ and $\text{Re} = 50{,}000 \div 2{,}100{,}000$) are accurately represented in the numerical model based on blade element theory. The thrust is aligned with aircraft centre of gravity.

A preliminary assessment of simulation accuracy in terms of energy balance budget is performed. Flight test data give evidence that for the cruise flight conditions ($U = 13{\cdot}5\text{ms}^{-1}$) the current drain from the battery is measured as $\Delta C = 47{\cdot}5 \pm 2{\cdot}5\text{mA·min}$. The simulation software predicts (for the same reference case) $\Delta C = 52{\cdot}5\text{mA·min}$, an acceptable approximation for the performance of the real vehicle. As a matter of fact, the ability to assess the performance of the controlled aircraft may allow an accurate prediction of mission endurance, a vital point for this family of mini-UAVs that usually fly with a very limited margin for energy storage.

The main performance analysis is based on the comparison of time-domain altitude and airspeed indicial response of the vehicle starting from cruise flight, replicating the typical mission for mini-UAVs i.e. tracking the assigned waypoints along flight segments at constant altitude and airspeed, usually selected step after step according to the mission plan.

The two autopilot flight modes are compared for both flight altitude and airspeed increments where the amplitude of the steps is set within a realistic range of values comparable with the typical corrective steps enforced by the autopilot during level flight[7]. Note that larger increments would induce the switch of autopilot from level flight mode to climb/descent control modes (at least during the transient phase).

In straight level flight (the small angles of attack assumption is also invoked), the increase of either airspeed or angle-of-attack induced by control actions (elevator angle δ_e or throttle χ) determine the sign of the function $f_1 = -Z - W$ that is equal to zero for level flight and it indicates

Figure 2. An example of mini-UAV (hand launch of MAVTech MH850).

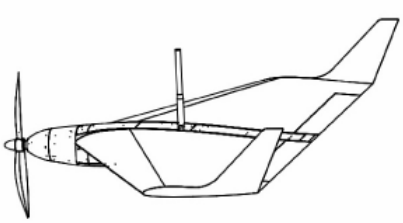

Figure 3. An example of mini-UAV (outer view of MAVTech MH850).

the transition to climbing or descending flight when positive or negative. If any aircraft increases the airspeed at constant angle-of-attack (assuming infinite longitudinal static stability) the consequence will be a climb and then a deceleration induced by larger drag. If throttle is not correctly compensated, the aircraft will decelerate progressively if $f_2 = T + X < 0$. If, differently, the angle-of-attack is increased/decreased at constant airspeed (i.e. through elevator control), the lift will overbalance or underbalance the weight of the aircraft ($f_1 = -Z-W$ positive or negative) producing a transition to climbing/descending flight. The angle-of-attack will also change the drag in a way to decelerate/accelerate the vehicle. Therefore, a correction of throttle is mandatory to balance the flight condition. The two mechanisms are superimposed during the flight and together they explain the altitude and airspeed variations encountered.

The response to a reference altitude variation (Δh = 10m) is presented in Fig. 3. Mode (1) exhibits a smooth altitude response combined with a fast airspeed oscillatory response, rapidly damped out after a short transient. Differently mode (2) provides a short term oscillatory altitude dynamics with reduced settling time and a more progressive airspeed response. Thrust (and consequently current) adapts to mode type accordingly (see Fig. 3). Note that thrust spikes induced by the derivative control term are not filtered by the simulator. Mode (2) is characterised by an immediate thrust (and current) overshoot for airspeed loss compensation. The comparison of excess power – measured as the difference between thrust and drag power – presented in Fig. 3 demonstrates that mode (1) acts through a progressive decrease of thrust power for constant drag power. Differently, mode (2) shows an initial dominant overshoot of thrust power combined with a decrease of drag power, followed by a visible power compensation as a consequence of thrust oscillation induced by airspeed stabilisation.

Table 1
The effect of autopilot mode setting on cumulative performance metrics
(Δh = 1 ÷ 10m – ΔT = 60s)

Δh (m)	ΔE (J)	Mode (1/2)	C (%)	ΔC (%)	ε_I (–)	ε_h (–)	ε_U (–)
1	9·5	1	1·814	0·017	1·000	1·000	1·000
		2	1·814	0·017	1·000	0·480	6·830
10	95	1	1·967	0·170	1·000	1·000	1·000
		2	1·975	0·177	1·004	0·640	6·534

The response to a reference airspeed increment (ΔU = 5ms^{-1}) is shown in Fig. 3. As expected, the airspeed of the vehicle when controlled in mode (1) rises very rapidly with an overshoot and some damped oscillations, reacting to elevator deflections. The loss of altitude is compensated with the progressive action of throttle over a longer settling time. On the other side, mode (2) enforces airspeed with quite a rapid reaction of the throttle that is superimposed to an altitude increase, neutralised over a longer transient. The required acceleration is obtained for mode (2) with a sharp thrust (and current) rise, as outlined in Fig. 3, and the excess of thrust power (see Fig. 3) over the increased drag power is shaped in a coherent manner for airspeed compensation in the very first phase after the commanded step.

The effect of autopilot mode setting on cumulative performance is estimated by means of the following parameters;

$$\varepsilon_I = \sum_{i=1}^{N} I_i \quad \varepsilon_h = \sum_{i=1}^{N} \| h_i - h_0 \| \quad \varepsilon_U = \sum_{i=1}^{N} \| (U_i - U_0) \| \qquad \ldots (7)$$

where the sampling time interval is the integration time step Δt = 0·001s. The parameters are normalised with respect to mode 1 (set to unity) and they are presented in Tab. 1 for the altitude step $\Delta h = 1 \div 10$m and in Tab. 2 for the airspeed step $\Delta U = 1 \div 5\text{ms}^{-1}$. The increments in altitude and airspeed are defined for similar steps of system's mechanical energy ΔE. The data show that the sampling time ΔT is large enough to obtain final steady state conditions ($\varepsilon_I \approx 1$). The elevator is a fast and precise type of control. As a matter of fact, mode (1) provides accurate tracking of airspeed (lower ε_U for all cases) as the airspeed is controlled by elevator deflection. Mode (2) tracks altitude with a limited error ε_h as a result of elevator feedback control. The use of throttle for the control of altitude for mode (1) or airspeed for mode (2) gives slower and less accurate tracking of the reference states. The acceleration of the vehicle requires a larger dissipation of battery charge (drag induced penalty) as demonstrated by the values of ΔC in Tab. 2 compared with the equivalent steady state increment of mechanical energy ΔE.

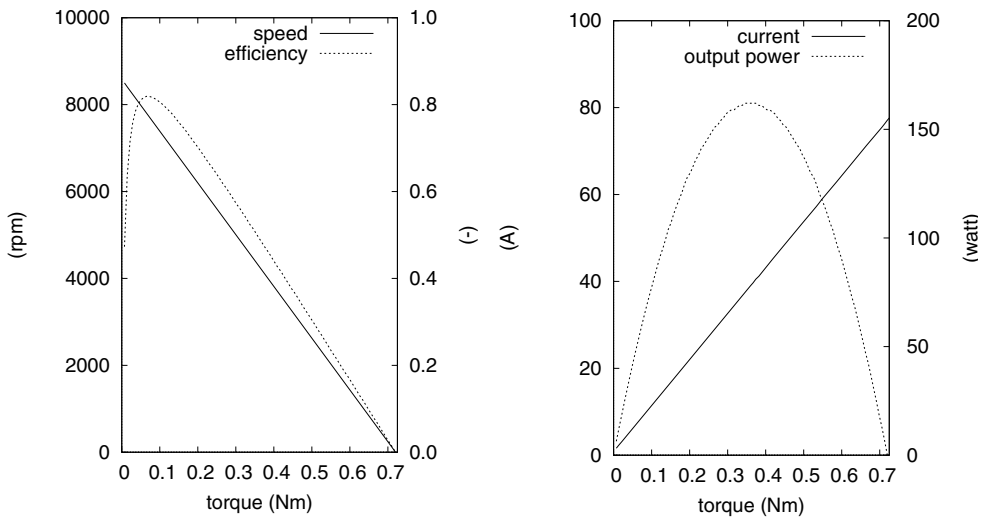

Figure 4. The electric motor characteristic curves (V_0 = 8·4V).

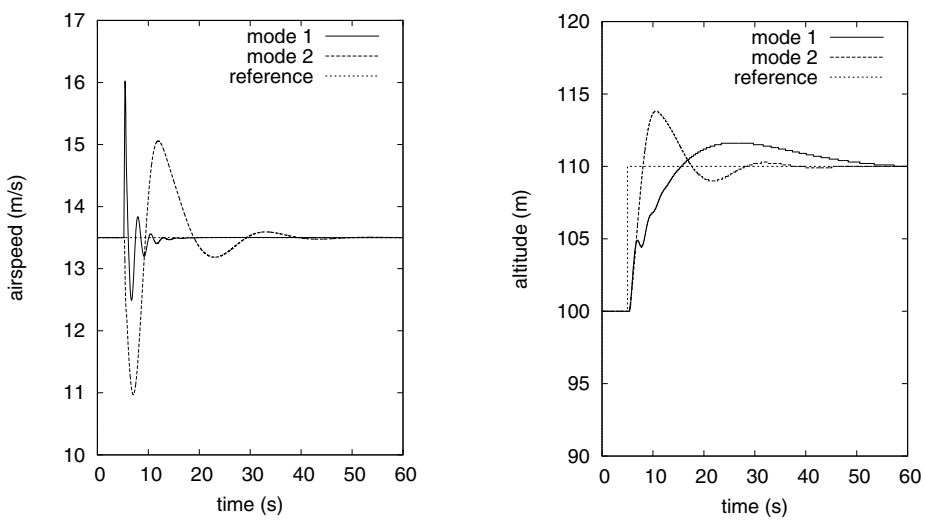

Figure 5. The response of the aerial vehicle to an altitude step command for the different autopilot modes (Δh = 10m).

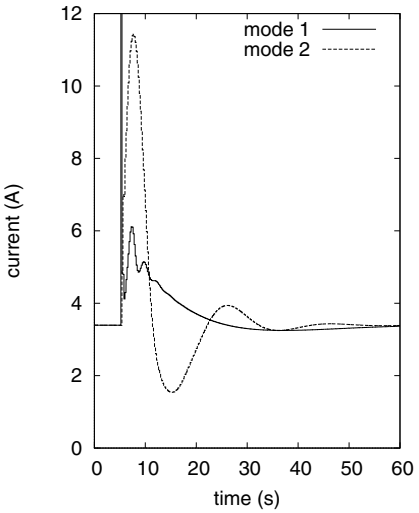

Figure 6. The response of the aerial vehicle to an altitude step command for the different autopilot modes (Δh = 10m).

Table 2
The effect of autopilot mode setting on cumulative performance metrics ($\Delta U = 1 \div 5 \text{ms}^{-1} - \Delta T = 60\text{s}$)

ΔU (ms^{-1})	ΔE (J)	Mode (1/2)	C (%)	ΔC (%)	ε_I (–)	ε_h (–)	ε_U (–)
1	13·6	1	1·865	0·068	1·000	1·000	1·000
		2	1·862	0·065	0·998	0·431	2·190
5	77·8	1	2·335	0·538	1·000	1·000	1·000
		2	2·292	0·495	0·981	0·290	1·745

4.0 CONCLUDING REMARKS

The present paper proposes a validated approach to include the relevant modelling elements in a comprehensive simulation tool reproducing some of the flight phases of a mini-UAV.

The propulsion system is represented by three sequential contributors (propeller, motor and battery pack) and their models are detailed and validated separately. Their dynamics is assumed to be at least one order of magnitude faster than the vehicle's response to commands. The overall mathematical representation of the vehicle is implemented in a numerical solver of the equations of motion including a detailed but compact database for aircraft aerodynamics.

The steady state current drain is compared with flight test data available for a reference mini-UAV configuration.

The effect of the autopilot control loops is included taking into account the update rate of the real digital implementation. Two different autopilot modes are considered: mode (1) in which elevator controls airspeed while throttle controls altitude, and mode (2) that performs the opposite type of control.

The energy balance budget and the dynamic response of the aircraft during the automatic flight are investigated, assessing the impact of autopilot configuration, such as altitude-airspeed holding

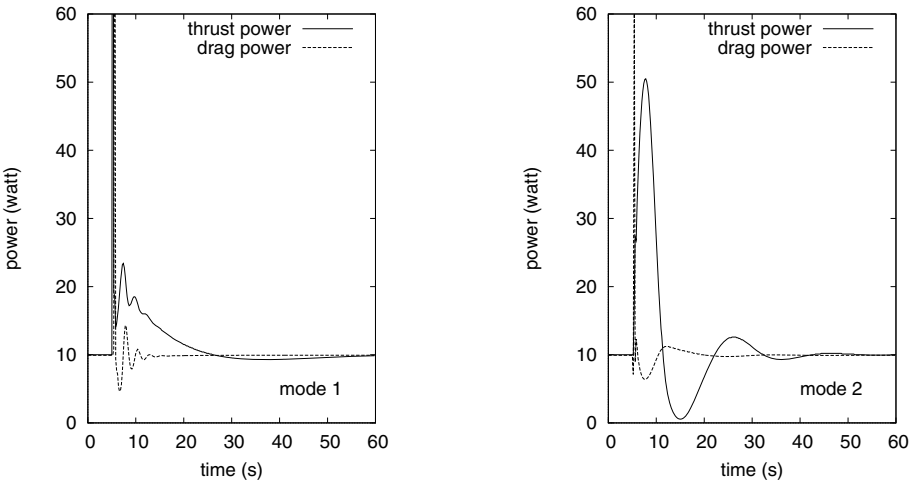

Figure 7. The response of the aerial vehicle to an altitude step command for the different autopilot modes (Δh = 10m).

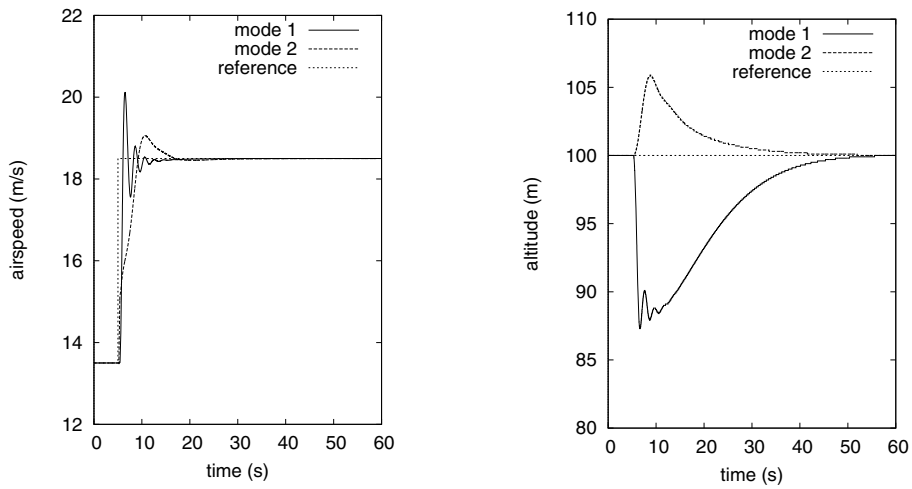

Figure 8. The response of the aerial vehicle to an altitude step command for the different autopilot modes (ΔU = 5ms^{-1}).

modes and suggesting a setting guideline for flight mode selection compatible with the features of commercial autopilots. The results are dependent on the aircraft configuration, such as where the propeller thrust line is located relative to the vehicle mass centre (for the present case the thrust is aligned with the centre of gravity). Moreover, the results would be also affected by control system gains. So the following conclusions cannot be generally extended but provide a guideline for the performance assessment of autopilot modes.

In the present case, mode (1) provides accurate tracking of airspeed (lower ε_U for all cases) as the airspeed is controlled by elevator deflection. Mode (2) tracks altitude with a limited error ε_h as a result of elevator feedback control. The use of throttle for the control of altitude for mode (1)

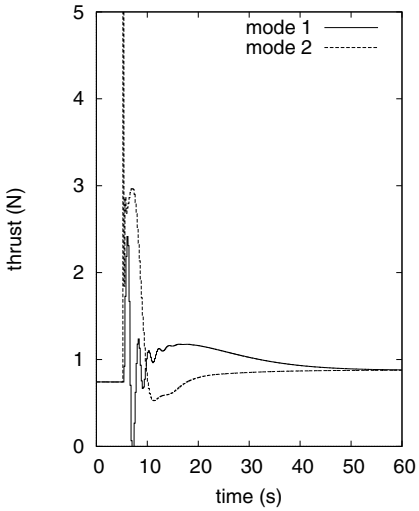

Figure 9. The response of the aerial vehicle to an altitude step command for the different autopilot modes (ΔU = 5ms^{-1}).

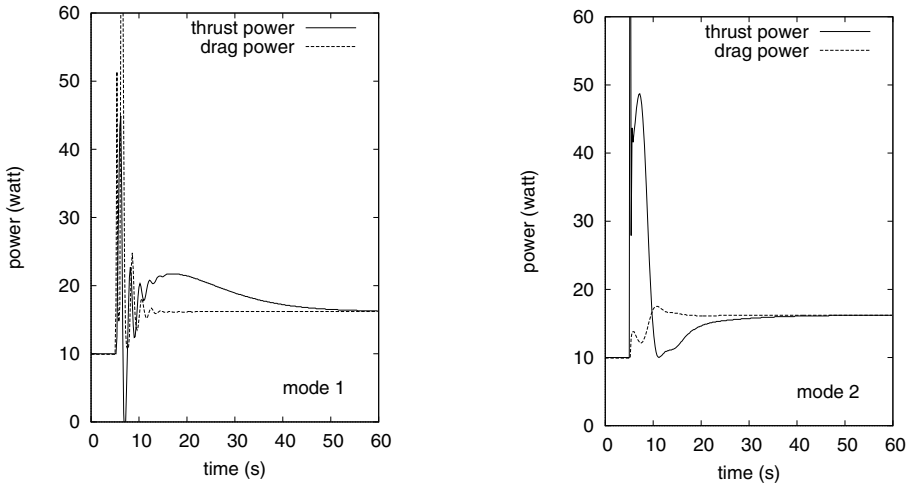

Figure 10. The response of the aerial vehicle to an altitude step command for the different autopilot modes (ΔU = 5ms^{-1}).

or airspeed for mode (2) gives slower and less accurate tracking of the reference states. Furthermore, the acceleration of the vehicle requires a larger dissipation of battery charge (drag induced penalty) as demonstrated by the values of ΔC in Tab. 2 compared with the equivalent steady state increment of mechanical energy ΔE.

As expected, a frequent update of the reference airspeed significantly reduces the available battery charge, suggesting to program the autopilot in a way to keep constant airspeed (as much as possible). Altitude changes cannot be obviously avoided but the selection between mode (1) and mode (2) should be driven by the required tracking accuracy in terms of airspeed or, alternatively, altitude, depending on both the type of sensors being used for the application and the required margin of separation from ground obstacles.

5.0 ACKNOWLEDGEMENTS

The author wishes to acknowledge the invaluable technical assistance given by the staff of MAVTech s.r.l. (www.mavtech.eu) and by Mr Paolo Marguerettaz and Mr Daniele Sartori.

REFERENCES

1. MÜLLER, T.M. *Fixed and Flapping Wing Aerodynamics for Micro Air Vehicle Applications*, AIAA Progress in Astronautics and Aeronautics Series, 2001.
2. MÜLLER, T.M., KELLOGG, T.J., IFJU, P.G. and SHKARAYEV, S.V. *Introduction to the Design of Fixed-Wing Micro Air Vehicles*, AIAA Education Series, 2007.
3. MUSIAL, M. *System Architecture of Small Autonomous UAVs*, VDM Verlag, 2008.
4. AUSTIN, R. *Unmanned Air Systems: UAV Design, Development and Deployment*, Wiley, 2010.
5. NONAMI, K., KENDOUL, F., SUZUKI, S., WANG, W. and NAKAZAWA, D. *Autonomous Flying Robots: Unmanned Aerial Vehicles and Micro Aerial Vehicles*, Springer, 2010.
6. BEARD, R.W. Small Unmanned Aircraft: Theory and Practice, Princeton University Press, 2012.
7. *Micropilot Autopilot Installation and Operation*, Micropilot, 2010.
8. CAPELLO, E., GUGLIERI, G. and QUAGLIOTTI, F. A Software Tool Mission Design and Autopilot Integration: an Application to Micro Aerial Vehicles, EUROSIW Conference, Edinburgh, Scotland, UK, 2008.
9. CAPELLO, E., GUGLIERI, G. and QUAGLIOTTI, F. UAVs and simulation: an experience on MAVs, *Aircraft Engineering and Aerospace Technology*, 2009, **81**, (1), pp 38-50.
10. ABRAMOWITZ, M. and STEGUN, I.A. *Handbook of Mathematical Functions with Formulas, Graphs, and Mathematical Tables*, Dover, 1972, p 896.
11. GLAUERT, H. *The Elements of Aerofoil and Airscrew Theory*, Cambridge University Press, 2011.
12. BEATY, H.W. and FINK, D.G. *Standard Handbook for Electrical Engineers*, McGraw-Hill Professional, 2006.
13. WILDI, T. *Electrical Machines, Drives and Power Systems*, Prentice Hall, 2006.
14. TYREUS, B.D. and LUYBEN, W.L. *Tuning PI Controllers for Integrator Dead Time Processes*, *Industrial and Engineering Chemistry Research*, 1992, **31**, (11), pp 2628-2631.
15. MARGUERETTAZ, P., SARTORI, D., GUGLIERI, G. and QUAGLIOTTI, F. Design and Development of Man-Portable Unmanned Aerial System for Alpine Surveillance Missions., UAS International Conference, Paris, France, 2010.
16. GUGLIERI, G., PRALIO, B. and QUAGLIOTTI, F. Flight control system design for a micro aerial vehicle, *Aircraft Engineering and Aerospace Technology*, **78**, (2), 2006, pp 87-97.
17. GUGLIERI, G., PRALIO, B. and QUAGLIOTTI, F. Design and Performance Analysis of a Micro Aerial Vehicle concept, 2nd AIAA Unmanned Unlimited Systems Technologies and Operations – Aerospace, Land, and Sea Conference, San Diego, USA, 2003.
18. WEISSINGER, J. The Lift Distribution of Swept Wings, NACA TM-1120, 1947.
19. Aircraft Configuration Interface Software Manual, Mavtech Report, www.mavtech.eu, 2006.